Role of all jet drops in mass transfer from bursting bubbles

Alexis Berny,[1,2] Luc Deike,[2,3] Thomas Séon,[1] and Stéphane Popinet[1]
[1]*Sorbonne Université, CNRS, UMR 7190, Institut Jean le Rond ∂'Alembert, F-75005 Paris, France*
[2]*Department of Mechanical and Aerospace Engineering, Princeton University, Princeton, New Jersey 08544, USA*
[3]*Princeton Environmental Institute, Princeton University, Princeton, New Jersey 08544, USA*

(Received 12 September 2019; accepted 13 February 2020; published 10 March 2020)

When a bubble bursts at the surface of a liquid, it creates a jet that may break up and produce jet droplets. This phenomenon has motivated numerous studies due to its multiple applications, from bubbles in a glass of champagne to ocean/atmosphere interactions. We simulate the bursting of a single bubble by direct numerical simulations of the axisymmetric two-phase liquid-gas Navier-Stokes equations. We describe the number, size, and velocity of all the ejected droplets, for a wide range of control parameters, defined as nondimensional numbers, the Laplace number which compares capillary and viscous forces and the Bond number which compares gravity and capillarity. The total vertical momentum of the ejected droplets is shown to follow a simple scaling relationship with a primary dependency on the Laplace number. Through a simple evaporation model, coupled with the dynamics obtained numerically, it is shown that all the jet droplets (up to 14) produced by the bursting event must be taken into account as they all contribute to the total amount of evaporated water. A simple scaling relationship is obtained for the total amount of evaporated water as a function of the bubble size and fluid properties. This relationship is an important step toward building a physics-based model of the ocean-atmosphere water vapor fluxes controlled by bubbles bursting at the surface.

DOI: 10.1103/PhysRevFluids.5.033605

I. INTRODUCTION

The production of droplets due to bubbles bursting at the surface of a liquid has long been considered as a fundamental mechanism controlling larger-scale fluxes between the liquid and the gas. This is particularly true in a geophysical context, with the pioneering studies on aerosol generation of Woodcock and Blanchard [1,2]. Blanchard was the first to measure the size of the droplets produced by a bursting bubble [3]. In a follow-up article [4] they estimated the height of the ejected droplets. The overall importance of this mechanism for large-scale atmospheric (bio)physics was further underlined by Blanchard and collaborators in subsequent articles [5,6]. After a relatively quiet interval, the topic was revived in the 1990s by the important experimental studies of Spiel, who obtained statistics on the number, sizes, and velocities of the droplets produced by bubbles bursting in water [7] and in salt water [8]. More recently, this process was also studied in the context of the spread of aroma of sparkling beverages, in particular champagne wine [9,10].

From a theoretical perspective, recent advances in the description of two-phase interfacial flows coupled with the development of accurate numerical methods have led to a much-improved understanding of the experimental measurements. The first direct numerical simulation of the axisymmetric bursting was carried out in our group in 2002 [11] and led to the discovery that the main parameter controlling the speed and size of the first-ejected droplet is the ratio of the surface tension and viscous forces (as estimated with the Laplace or Ohnesorge number).

More specifically, and somewhat counterintuitively, this study showed that there exists an optimal viscosity (corresponding to a Laplace number around 1000) for which jet focusing is most efficient and leads to the ejection of very fast, tiny droplets (several tens of m/s for air in water). In the meantime, the use of high-speed cameras has also led to very detailed and accurate experimental data on the size and velocity of the first droplet [12–14]. These experimental data sets, combined with high-resolution numerical results obtained using the methods developed in our group [15,16], now give a very consistent picture of the behavior of the jet focusing and first-ejected droplet [17,18], for the whole range of controlling parameters. These results have been used very recently by Gañán-Calvo [19,20] and Gordillo and Rodriguez-Rodriguez [21] to propose scaling models able to describe accurately the size and velocity of the first droplet, for Laplace numbers larger than the optimal value. Lai *et al.* [22] reconciled such scalings with the cavity collapse and jet formation described by inviscid inertio-capillary self-similar solutions, therefore providing universal functional form for the dynamical process up to the ejection of the first drop.

While the behavior of the first-ejected droplet can thus be considered as relatively well understood, the number, sizes, and speeds of subsequent droplets are much more poorly documented. From our knowledge, the only experimental data sets were obtained by Spiel [7,8] for air bubbles in water and saltwater. Numerical results on subsequent droplets are also scarce. When considering the integrated flux due to the entire history of bubble bursting, there is no objective reason to assume that the dominant role is played by the first-ejected droplet. This observation was the motivation behind Spiel's 1994 experimental study.

The primary aim of the present article is to understand the behavior of all the droplets produced, in the perspective of being able to explain and predict the resulting fluxes due to the entire bubble bursting process. The main result used to achieve this goal is an extensive data set obtained through direct numerical simulations. After a brief summary of the numerical setup (Sec. II), we describe in detail the process of multiple droplet generation by a bursting bubble. The numerical setup is validated through a systematic study of the first droplet behavior, compared to experimental and numerical results available from previous work (Sec. III). Section IV constitutes the bulk of the study with systematic data on the number, sizes, and speeds of all droplets produced and an interpretation of these results. The resulting vertical momentum is then discussed. Finally, in Sec. V we show how these data can be used to build a semiempirical model able to explain and predict the total amount of water vapor transferred from water to air as a function of the size of the bursting air bubble.

II. NUMERICAL METHOD

We consider two Newtonian, immiscible fluids separated by an interface with constant surface tension. We note ρ_i and μ_i the density and viscosity of fluid i. γ stands for the surface tension coefficient and g is the acceleration of gravity. The radius of the bursting bubble is denoted R_b. Four dimensionless numbers describe the problem fully. We set the density and viscosity ratios to $\rho_\mathrm{liq}/\rho_\mathrm{gaz} = 998$ and $\mu_\mathrm{liq}/\mu_\mathrm{gaz} = 55$, which is close to the values for air and water. For the two remaining numbers, we chose the Laplace number, La, which compares the capillary forces with the viscous forces, and the Bond number, Bo, which compares the gravitational forces with the capillary forces. They are defined as

$$\mathrm{La} = \frac{\rho_\mathrm{liq}\gamma R_\mathrm{b}}{\mu_\mathrm{liq}^2}, \tag{1}$$

$$\mathrm{Bo} = \frac{\rho_\mathrm{liq} g R_\mathrm{b}^2}{\gamma}. \tag{2}$$

The initial condition is given by the shape of a bubble at rest below an horizontal interface. This temporary equilibrium shape is due to the long drainage time of the thin liquid film separating the top of the bubble from the outside gas phase, compared to the time taken to reach balance between surface tension forces and buoyancy. This balance of forces is described by the Young-Laplace

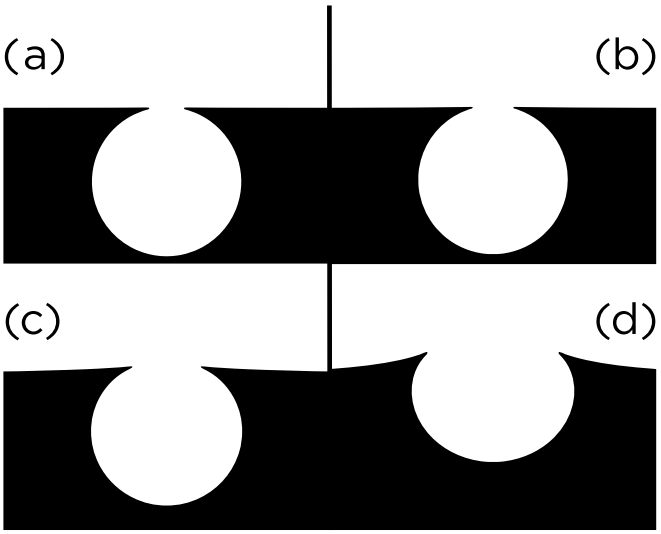

FIG. 1. Shapes of a bubble at rest used to initialize the simulations. The shapes are obtained by solving the Young-Laplace equation for varying Bond numbers: (a) Bo = 0.00094; (b) Bo = 0.0088; (c) Bo = 0.074; (d) Bo = 0.63.

equation [12,23], which we solve numerically [24]. Figure 1 represents the different bubble shapes obtained when varying the Bond number (which is the only relevant parameter for the Young-Laplace equation).

The 2D axisymmetric simulations are performed using the Basilisk open-source library [25], solving the two-phase incompressible Navier-Stokes equations with surface tension. The principle of the method and the numerical schemes are close to that used in our previous work [17,22,26–28] using the Gerris solver [15,16], but their implementation benefits from the various improvements brought by the new Basilisk framework, in particular regarding the mesh adaptation methods. The adaptive mesh is critical to the success of these simulations as it allows fast solution for discretizations with an equivalent resolution of up to 4^{14} grid points.

While gravity is always taken into account to obtain the initial shape, its action is not taken into account in the dynamics, for Bond numbers below 0.1. This approximation is justified as will be shown later when validating with previous results.

Figure 2 summarizes a typical sequence of droplet generation for a Bond and Laplace number of Bo = 0.0094 and La = 4847, respectively. The bottom three panels give the axisymmetric profiles of the free surface and ejected droplets. The top graph illustrates the evolution with time of the vertical position of the tip of the jet (black) and of each generated droplets (colors), the vertical position normalized by the bubble radius R_b. The time is normalized by the capillary timescale $t_c = \sqrt{\rho_\mathrm{liq} R_\mathrm{b}^3/\gamma}$. The position of the center of mass of the droplets is obtained by integrating numerically over each subset of contiguous grid points, separated by the gas phase. The mass of each droplet is also obtained in this way and is conserved accurately during their evolution.

Using this summary data, we can extract automatically the initial ejection speed, V, and volume of each generated droplet. We define the capillary number:

$$\mathrm{Ca} = \frac{V \mu_\mathrm{liq}}{\gamma}, \tag{3}$$

which compares the jet (or droplets) velocity with the visco-capillary velocity γ/μ_liq. Each droplet velocity will be denoted Ca_{d_i} with i the index of the droplet (1 for the first droplet, 2 for the second, etc.).

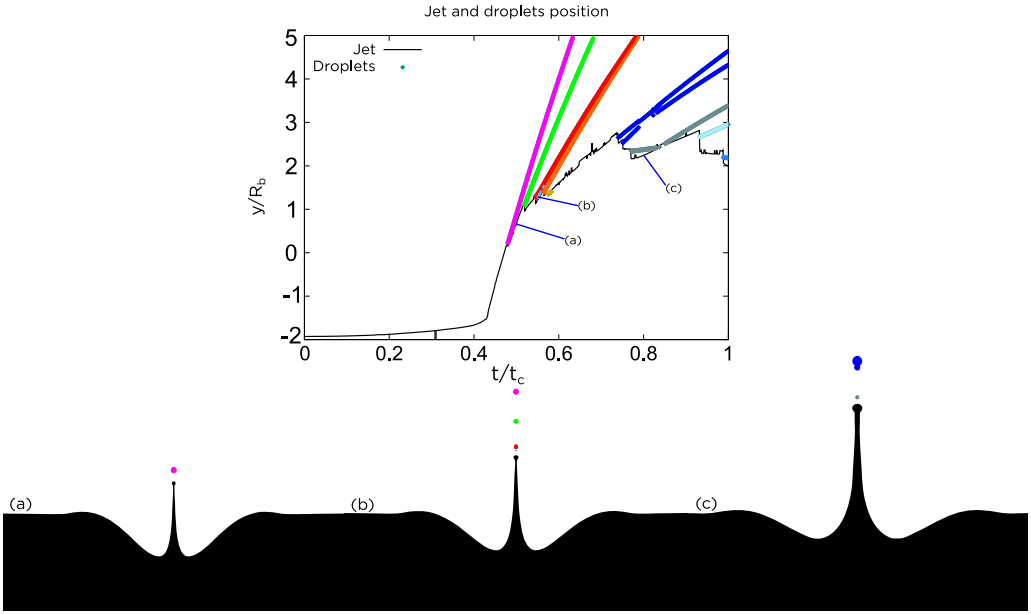

FIG. 2. Jet formation and ejection of multiple droplets by a bursting bubble for Bo = 0.0094 and La = 4847. Top graph: Evolution with time of the vertical position of the jet tip (black) and droplets (colors). Time is normalized by the capillary timescale $t_c = \sqrt{\rho_{\text{liq}} R_b^3/\gamma}$. Bottom three panels: Axisymmetric profiles of the jet and droplets at the three different times (a), (b), and (c) indicated in the top graph.

III. FIRST DROP DYNAMIC STUDY

A. Velocity of the first droplet

As underlined in the introduction, the velocity of the first-ejected droplet, as a function of the control parameters, is now well known, both experimentally and numerically. To validate our numerical setup, as well as the algorithms in Basilisk, we first compare our results to previous numerical and experimental data. As pointed out in Deike *et al.* [17], some care needs to be taken in the definition of the ejection speed in order to obtain meaningful comparisons. We use the speed of the droplet just after its formation. This is comparable to the plateau in the jet velocity used in Deike *et al.* [17].

Figure 3 illustrates the evolution of the first droplet dimensionless velocity Ca_{d_1} for a range of Laplace (500 to 500 000) and Bond numbers (0.94×10^{-3} to 1). Both our data (filled diamonds) and data from Deike *et al.* [17] (empty triangles) are represented. The data from Deike *et al.* were validated against experimental data from Ghabache *et al.* [12]. Good agreement between the two data sets is obtained for the whole range of Laplace and Bond numbers. A maximum in ejection speed of around three times the visco-capillary velocity is obtained for a Laplace number around 1000 at low Bond numbers. At higher Bond numbers this maximum decreases (down to around 0.4 for Bo = 0.64) and the value of the corresponding optimal Laplace number increases (up to around 4000 for Bo = 0.64).

Gañàn-Calvo [19] proposed a scaling law for the velocity of the first drop based on a balance of the momentum equation terms during curvature reversal, which leads to the black curve in Fig. 3(a), given by

$$\text{Ca} = k_v[\text{La}(\text{La}_\star^{-1/2} - \text{La}^{-1/2})]^{-3/4}, \tag{4}$$

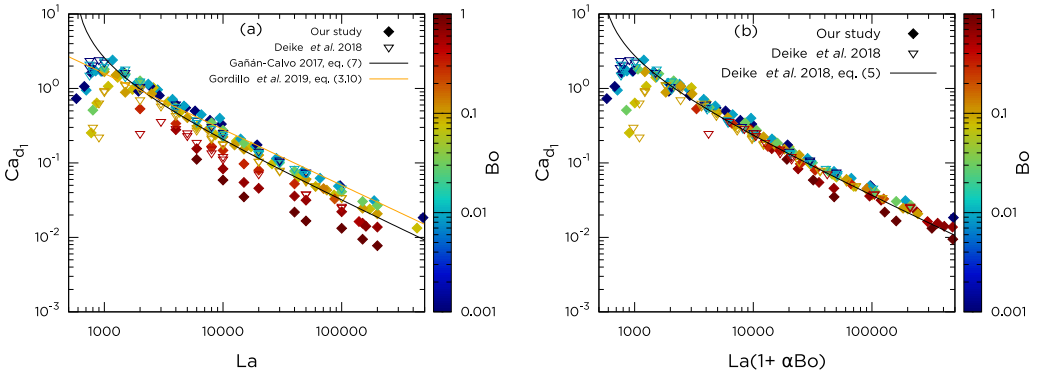

FIG. 3. (a) Dimensionless velocity of the first drop Ca as a function of the Laplace number. Data from Deike *et al.* [17] (open triangles) and our numerical data (plain diamonds). The color scale indicates the Bond number of the simulation, varying from 10^{-3} to 1. The scaling law proposed by Gañàn-Calvo under the no-gravity assumption [19], given by Eq. (4), and its asymptotic scaling, $\mathrm{Ca} \propto \mathrm{La}^{-3/4}$ are shown in solid and dashed lines, respectively. An equivalent scaling discussed in Ref. [21] is indicated. As reported by Deike *et al.* [17], gravity starts to induce a correction in the first drop velocity for $\mathrm{Bo} > 0.1$. (b) Rescaled data set using the empirical relation proposed by Deike *et al.* [17], given by Eq. (5), and adapted from Gañàn-Calvo [19]. Our results are fully consistent with existing literature and confirm that the jet velocity before droplet ejection measured in Ref. [17] is similar to the first droplet ejection velocity.

where $\mathrm{La}_\star \approx 500$ is the critical value of the Laplace number below which no droplet is produced and $k_v \approx 16$ is a nondimensional coefficient fitted to the data. Note that gravity is not taken into account in this scaling ($\mathrm{Bo} = 0$).

Gordillo and Rodriguez-Rodriguez [21] discussed an alternative argument for the formation velocity of the jet at the bottom of the cavity, considering the focusing of the capillary waves. This result is compatible with the present data and equivalent in the asymptotic limit $\mathrm{La} \gg 1000$, also indicated on Fig. 3(a), as it reads $\mathrm{Ca} \sim \mathrm{La}^{-3/4}$.

The effect of gravity is taken into account empirically in the rescaling of the x axis proposed by Deike *et al.* (2018), which can be written

$$\mathrm{Ca} = k_{v\mathrm{Deike}}(1 + \alpha \mathrm{Bo})^{-3/4}\mathrm{La}^{-3/4}(\mathrm{La}_*^{-1/2} - \mathrm{La}^{-1/2})^{-3/4}, \tag{5}$$

where α is a nondimensional coefficient. We fitted $\alpha = 2.2$ and $k_{v\mathrm{Deike}} = 19$ to the data to obtain the rescaling in Fig. 3(b). The rescaling seems to work reasonably well. Note that Ref. [20] discusses another scaling that accounts for the effect of the gravity and appears fully compatible with the present empirical formula.

B. Size of the first droplet

We now study the size of the first droplet as a function of the control parameters. The *droplet* Laplace number is defined as

$$\mathrm{La}_\mathrm{d} = \frac{\rho \gamma R_\mathrm{d}}{\mu^2} \tag{6}$$

with R_d the droplet radius. The size of the i ejected droplet will then be denoted La_{d_i}. Figure 4 illustrates the dependency of $\mathrm{La}_{\mathrm{d}_1}$ on the control parameters (bubble Laplace number La and Bond number Bo). The evolution with Laplace number mirrors that of the droplet velocity, with a minimum obtained for the "optimal" Laplace number around 1000. In contrast with the droplet velocity, though, gravity seems to have a minimal influence on the size of the first droplet. All experimental and numerical data sets are remarkably consistent. Gañàn-Calvo [19] proposed the

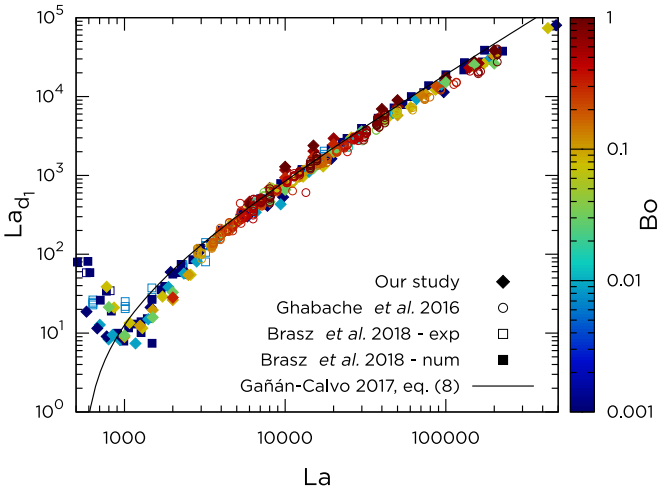

FIG. 4. Droplet Laplace number La_{d_1} as a function of the bubble Laplace number La, with Bo color-coded. The filled diamonds are data from the present study. The open circles are experimental data from Ref. [14]. The filled squares are numerical data from Ref. [18], and the empty squares are experimental data from the same study. An excellent match between all data is observed for all La and Bo. The black curve is the scaling law from Ref. [19], Eq. (7), which describes well the data for La $>$ 1000.

following scaling:

$$\mathrm{La}_{d_1} = k_r \left[\sqrt{\mathrm{La}} \left(\sqrt{\frac{\mathrm{La}}{\mathrm{La}_*}} - 1 \right) \right]^{5/4}, \tag{7}$$

where k_r is a nondimensional coefficient fitted to the data. This relationship described the data extremely well for Laplace numbers greater than the optimal value (1000), while not capturing the behavior below La $=$ 1000. We emphasize the excellent match between the numerical and the experimental data from various groups [14,18] for the full range of Laplace and Bond numbers. This further confirms the clear understanding on the size of the first-ejected droplet for Laplace numbers above 1000 and validates our numerical setup against previous results. Note, however, that a deeper understanding of the physics of the entire ejection process is still needed to correct the limitations observed in the velocity and size models for low Laplace numbers, as pointed out in Ref. [29]. We now move on to a general study of all the droplets.

IV. A SYSTEMATIC STUDY ON ALL THE DROPLETS

Using the same simulations as presented in the previous section we now characterize all the droplets produced by a bursting bubble.

A. Number of droplets

Figure 5(a) shows the number (color-coded) of droplets produced by the jet, as a function of the Laplace and Bond numbers. The dashed line on the left delimits the range of (La, Bo) for which no droplets are produced. This no-droplet limit is in agreement with the results of Walls *et al.* [31] and Deike *et al.* [17], with no droplets for La $<$ $\mathrm{La}_* \approx 500$ and a Bond number dependency of this boundary for Bo $>$ 0.1. In the range of droplet production, we observe between 1 and 14 droplets being ejected depending on the Laplace and Bond numbers. The maximum number of droplet (14) is obtained close to the optimal Laplace number (La between 1000 and 2000) and for the smallest

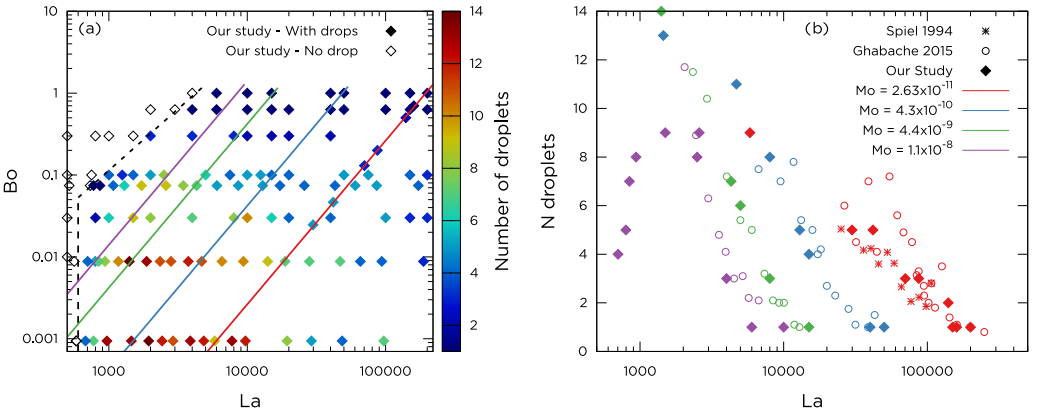

FIG. 5. (a) Number of droplets (color-coded) as a function of the Laplace and Bond numbers. No droplets are formed for La < 500 at low Bond number and with a Bond number dependency for Bo > 0.1, Bo $\propto$ La$^{3/2}$. The colored lines correspond to the constant Morton numbers of the figure on the right. The red line stands for Mo $= 2.63 \times 10^{-11}$ (pure water), the blue one stands for Mo $= 4.3 \times 10^{-10}$ (solution of 89.5% of water and 10.5% of ethanol), the green one stands for Mo $= 4.4 \times 10^{-9}$ (66.6% of water, 7.6% of ethanol and 25.5% of glycerin), and the purple one stands for Mo $= 1.1 \times 10^{-8}$ (55.3% of water, 4.9% of ethanol and 39.8% of glycerin). (b) Number of droplets as a function of the bubble Laplace number, for the constant Morton numbers indicated in the color-coded legend. Numerical (plain diamonds) and experimental results are represented (empty circles [30] and stars [7]). Good agreement is achieved between experimental and numerical data.

Bond numbers, which coincides with the fastest jet and smallest first droplet. The number of ejected droplet then decreases with increasing Bond number and increasing Laplace number.

To compare our numerical results with experimental data, we consider data sets for four different Morton numbers, defined as $\mathrm{Mo} = \mathrm{Bo}\,\mathrm{La}^{-2} = \frac{g\mu_{\mathrm{liq}}^4}{\rho_{\mathrm{liq}}\gamma^3}$. The Morton number is constant for a given liquid in laboratory experiments as it is set by the liquid properties only, namely, the viscosity, density, and surface tension coefficients. Figure 5(b) illustrates the corresponding dependencies of the number of droplets as a function of Laplace number for various solutions of water/glycerin/ethanol considered by Ghabache [30] and Spiel [7]. Both experimental (empty circles and crosses) and numerical (plain diamonds) results are displayed. Given the intrinsically variable nature of the phenomenon, the agreement between experiments and numerical results is remarkable. This plot confirms that the maximum number of ejected droplet is observed for the optimal Laplace number (faster and thinner jet) and decreases with increasing Laplace number. Note that, to the best of our knowledge [29], there is no theoretical understanding of the number of ejected droplets as a function of the Laplace and Bond numbers.

B. Velocity of the droplets

Within our range of control parameters, between $i = 0$ and 14 droplets are ejected when a bubble bursts. We now focus on the ejection velocity of the four droplets following the first one, namely $i = 2$ to 5, shown in Fig. 6 (left column) as functions of the bubble Laplace and Bond numbers. The scaling relation of Gañàn-Calvo [19], Eq. (4), describing the velocity of the first droplet ($n = 1$) at small Bond numbers is indicated for comparison in each panel. All droplets follow a trend similar to that of the first droplet, but with an increasing scatter as the droplet number is increased. Increasing the Bond number tends to decrease the velocity of the droplets and even suppress the creation of droplets entirely for large enough values (which explains the absence of red symbols on the bottom two rows). The large fluctuations in velocity obtained for droplets 4 and 5 (as well as subsequent

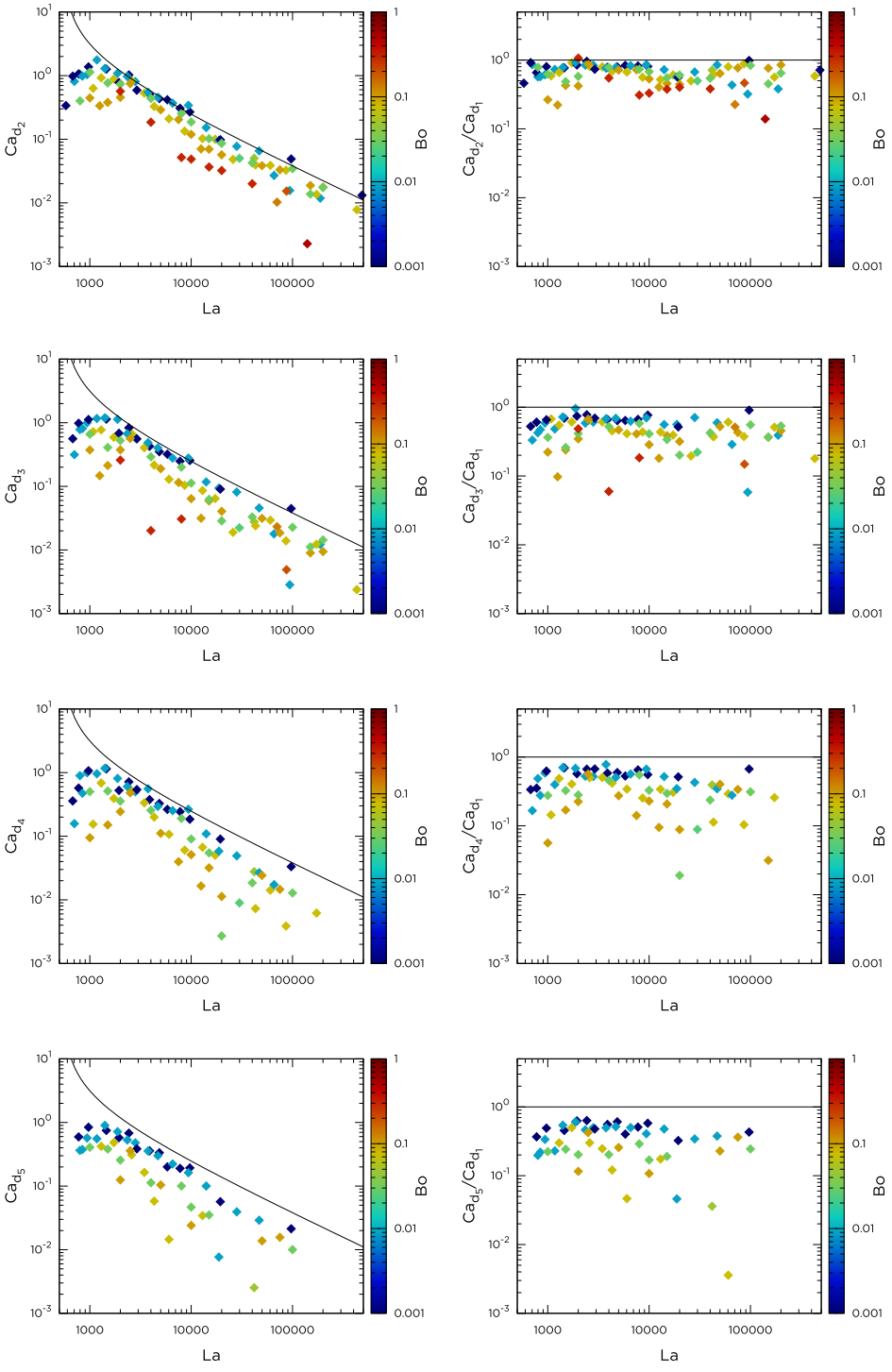

FIG. 6. (Left column) Dimensionless velocity, Ca_{d_i}, of droplets number $i = 2$ to 5 (top to bottom) as functions of the Laplace and Bond numbers (color-coded). The solid line reproduces the scaling relation of [19] for the first droplet, under the vanishing Bond number assumption. (Right column) Ratio of the dimensionless velocity of droplets number $i = 2$ to 5 (top to bottom) to the velocity of the first droplet Ca_{d_1}.

droplets not shown here) are a sign of the very nonlinear nature of the mechanisms producing these droplets. Preliminary studies have revealed, not unexpectedly, possible bifurcations between multiple states, which requires a detailed statistical analysis, as already suggested by Spiel [7]. This greatly complicates the analysis and detailed study of the breakup phenomenon and will be the topic of a follow-up article.

Figure 6 (right column) displays the ejection velocity of the same droplets as in the left column ($i = 2$ to 5), normalized by the velocity of the first one. These plots confirm that the velocity of the droplet i follows a similar trend to that of the first droplet and also shows that the ejection velocity tends to decrease as i increases.

C. Size of the droplets

Figure 7 (left column) presents the nondimensionalized size of the drops $n = 2$ to 5, expressed as a droplet Laplace number, La_d, as a function of the bubble Laplace number La for the whole range of Bond numbers (color-coded). The scaling relation of Gañàn-Calvo [19], Eq. (7), that describes the size of the first droplet ($n = 1$) for any Bond number (see Fig. 4) is given for comparison. The general trends are similar to those for the droplet velocities: An overall dependency on the Laplace number matching that for the first droplet, increasing scatter as the droplet index is increased, and a slight increase in droplet size with increasing Bond number. As for velocity, a statistical study of the size fluctuations would be necessary to properly quantify the variance.

The ratio of droplet size to the size of the first droplet, Fig. 7(right column), reveals that close to the optimal Laplace number ($\mathrm{La} \approx 1000$), subsequent droplets are significantly larger than the first droplet, which suggests that the finite-time curvature singularity approached by the collapsing bubble [11,12,17,18] no longer influences the drop size selection process.

D. Total vertical momentum

The primary motivation for studying the behavior of all the jet droplets is the estimation of the total transfer of momentum, heat, and eventually mass induced by the bursting of a single bubble [32]. Indeed, combining this information with statistical estimates (i.e., distributions) of bubble production, obtained from studies of, e.g., breaking waves (and their statistical distributions), could then be used to derive the large-scale fluxes controlling the coupled ocean-atmosphere system [33]. In this section we focus on the vertical momentum transferred from a bubble bursting via the drop ejection.

The total vertical momentum induced by bubble bursting is one of the potential candidates to explain the observed reduction of the air-sea drag coefficient in hurricane-force winds [32]. We combine the information on the droplet size and velocity to discuss the total vertical momentum related to jet droplets. We start by considering the nondimensional vertical momentum associated with the first droplet, e.g., $F^m_{d_1} = \frac{V_{d_1}}{\sqrt{\gamma/(\rho_{\mathrm{liq}}R)}}\left(\frac{R_{d_1}}{R}\right)^3$, shown in Fig. 8(a), where the droplet radius of the ith droplet is made nondimensional by the bubble radius, and the velocity of the ith droplet is made nondimensional by $\sqrt{\gamma/(\rho_{\mathrm{liq}}R)}$ naturally coming from the characteristic timescale t_c. We can combine the two scalings proposed by Gañàn-Calvo [19], Eqs. (4) and (7), and obtain

$$F^m_{d_1} = \frac{V_{d_1}}{\sqrt{\gamma/(\rho_{\mathrm{liq}}R)}}\left(\frac{R_{d_1}}{R}\right)^3 = k_d^3 k_v [\mathrm{La}(\mathrm{La}_\star^{-1/2} - \mathrm{La}^{-1/2})]^3 \mathrm{La}^{-5/2}. \tag{8}$$

The scaling in Eq. (8) is plotted with a black line in Fig. 8(a). As expected, the data for the first droplet follow this prediction relatively well for $\mathrm{La} > 5000$ since the data combine the scalings for the velocity and size, which closely match the numerical (and experimental) data. The effect of the Bond number is negligible, since the momentum scales like $\mathrm{La}^3_{d_1}\mathrm{Ca}_{d_1}$, and the droplet size/volume is almost independent from the Bond number, while the droplet velocity has only a weak dependence on the Bond number. The theoretical scaling fails to describe the data close to $\mathrm{La} = 1000$, which

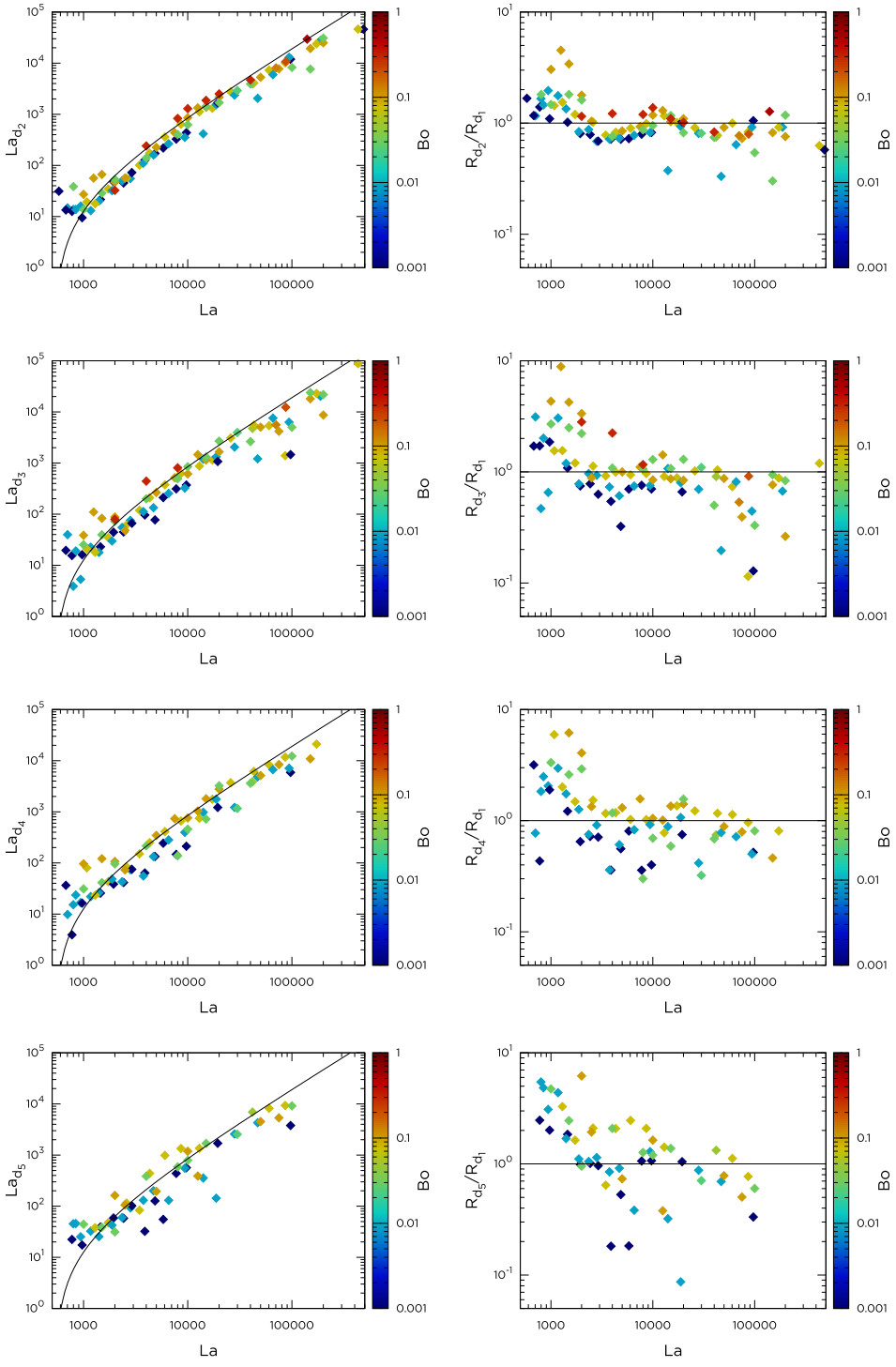

FIG. 7. (Left column) Sizes of the droplets $i = 2$ to 5 (top to bottom), La_{d_i} as functions of the bubble Laplace number, La, and Bond number (color-coded). The black line is the scaling relation Eq. (7) for the size of the first droplet, from [19]. (right column) Ratio of the size of droplets $i = 2$ to 5 to the size of the first droplet.

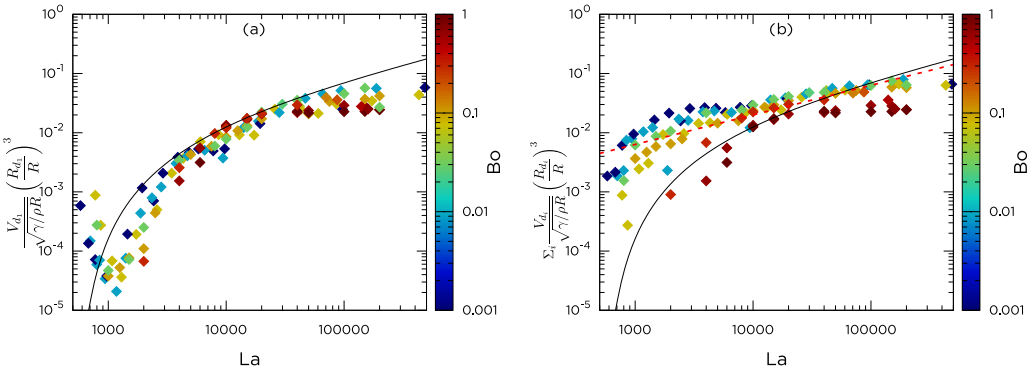

FIG. 8. (a) Nondimensional vertical momentum, defined as $R_{d_1}^3 V_{d_1}$ for the first-ejected droplet together with the scaling prediction [Eq. (8)] obtained by combining the scalings for the first droplet velocity [Eq. (4)] and size [Eq. (7)]. (b) Total vertical momentum for all the ejected droplets, $F^m_{\text{total}} = \sum_i R_{d_i}^3 V_{d_i}$. The asymptotic scaling $F^m_{\text{total}} \propto \text{La}^{1/2}$ is indicated by the red dashed line. The scaling of the first droplet is displayed with the black continuous line, which shows that the contributions of all droplets must be taken into account.

is a consequence of the limitation of the scaling near the optimal point. The mismatch at that point appears to be much higher compared to the one from Fig. 4, due to the fact that it scales in R^3, which increases the apparent difference on a log scale. Note that close to $\text{La} = 1000$, the ability of Gañán-Calvo's theoretical scaling to capture the correct velocity and size of the droplet relies on fitting coefficients, adjusted to a larger data set, while by construction it cannot capture the physics for $\text{La} < 1000$. To address this limitation, Gordillo and colleagues [21,34] proposed a different scaling law close to $\text{La} = 1000$, based on the collapse dynamics due to the focusing of the capillary waves, which also contains two fitting coefficients, the behavior for $\text{La} < 1000$ being described by yet another physical argument. These uncertainties in the precise mechanism around $\text{La} = 1000$, and variations in the fitting coefficients, explain the mismatch between the empirical data (either our numerical data or experimental data described in the papers cited above) and the scaling relationships for both the size of the first drop and its velocity. Further discussion is provided in Ref. [29].

We now consider the total vertical momentum, $F^m_{\text{total}} = \sum_i F^m_{d_i}$, with $F^m_{d_i}$ the vertical momentum for droplet number i normalized in a similar way as before. Figure 8(b) shows F^m_{total} as a function of the Laplace and Bond numbers. The influence of the Bond number is now more apparent, with an overall decreasing vertical momentum for increasing Bond number. This effect is clear for the highest Bond numbers ($\text{Bo} > 0.5$) and close to the optimal Laplace number, $\text{La} \approx 1000$, which can be attributed to the large differences in number of ejected droplets (see Fig. 5) combined with the relatively large droplet size for $i > 1$ (see Fig. 7) in this range of control parameter.

Remarkably, by summing the vertical momentum of all the droplets, the data align along a line over almost the full range of Laplace numbers, reasonably well approximated by $F^m_{\text{total}} \propto \text{La}^{1/2}$, represented by the red dashed line. This relation is the asymptotic scaling at high Laplace number of eq. (8). The singular behavior close to $\text{La} = 1000$ is smoothed out by the large number of droplets being ejected and by their large size. At low enough Laplace numbers, viscous dissipation causes a decrease in the total vertical momentum, and this trend is visible in Fig. 8(b) for $\text{La} < 1000$. This simple scaling can be combined with bubble distribution in order to obtain an estimation of the effects of spray on the air-sea momentum flux, for instance.

V. EVAPORATION OF THE DROPLETS

The large majority of previous studies on bubble bursting considered only the first droplet [11,14,18,20], arguing that the influence of following droplets might be negligible in the evaporation

process [13]. Here we obtained the size and the velocity for all the droplets, which was not previously reported in the literature. The results presented in the previous sections cast doubt on this assumption. Indeed, while the ejection velocity decreases quickly with droplet number, droplet sizes can be up to 10 times larger than that of the first droplet. With the number, velocity, and size of all the ejected droplets, we can now consider an evaporation model taking into account all the droplets generated by a bubble bursting and, consequently, estimate the total amount of liquid transferred from the droplets to the air by evaporation during a bubble bursting event.

A. A simple evaporation model

We consider the trajectory of a droplet in still air while taking into account the drag, the action of gravity, and the loss of mass due to the evaporation. The model we use has been fully described by Ghabache *et al.* [13] and compared successfully for the first-ejected drop to laboratory data. The model assumes immediate thermal equilibrium between the water and air phases once droplets are ejected. The ejected droplet follows an essentially ballistic trajectory (with drag corrections), and its flight time is thus controlled mainly by its initial velocity and gravity (i.e., Bond number).

The initial conditions for each ejected droplet are given by the results discussed earlier in the paper, namely, the ejection size and velocity of the droplets. The evaporation model then consists on the following coupled system, solving for the time evolution of each droplet radius $r_d(t)$ and velocity $v_d(t)$,

$$\frac{4}{3}\rho_l \pi r_d^3 \frac{\partial v_d}{\partial t} = -\frac{1}{2}\rho_{\text{air}} \pi r_d^2 v_d^2 C_D - \frac{4}{3}\pi \rho_l r_d^3 g, \tag{9}$$

$$\frac{\partial r_d^2}{\partial t} = -2 j_0 \left(1 + 0.3 \text{Sc}^{\frac{1}{3}} \text{Re}^{\frac{1}{2}}\right), \tag{10}$$

with C_D the drag coefficient of the droplet, $\text{Sc} = \frac{\mu_{\text{air}}}{\rho_{\text{air}} D}$ the Schmidt number, and $\text{Re} = \frac{\rho_{\text{air}} v_d r_d}{\mu_{\text{air}}}$ the Reynolds number. D is the diffusion coefficient of vapor in air, and j_0 is the evaporation parameter [35,36].

Equation (9) describes the evolution of the velocity of the droplet. Here C_D is the drag coefficient on a rigid sphere, in a steady motion. The Reynolds number of the ejected droplets ranges from zero to a hundred. Therefore we cannot use the Stokes approximation for drag forces on a sphere. Empirical studies approximates the drag coefficient as a function of the Reynolds number [37], and we use $C_D = \frac{24}{\text{Re}}(1 + 0.15\,\text{Re}^{0.687})$ valid for $\text{Re} < 800$ for solid spheres in the air [38].

Equation (10) describes the evolution of the radius of the droplet under quasisteady conditions. Since we consider low gas temperature (20 °C), we assume that the evaporation parameter j_0 is driven only by diffusion. This leads to $j_0 = \frac{\rho_{\text{air}}}{\rho_l} D(Y_{\text{vap}}^{\text{surf}} - Y_{\text{vap}}^{\infty})$, neglecting the Stefan flow [14,35]. We define Y_{vap} as the mass fraction of the vapor in the air: $Y_{\text{vap}} = \frac{\rho_{\text{vap}}}{\rho_{\text{air}}}$. Its value at the surface and in the far-field are considered. Equation (10) is derived using the assumption that the mass transfer may be modeled as occurring by diffusion within a spherical shell of thickness $r_d/(0.3\,\text{Sc}^{1/3}\text{Re}^{1/2})$. As a consequence, it is the combination of the d^2 law for the evaporation of a motionless droplet in air, which follows the equation $\frac{dr_d^2}{dt} = -2j_0$ [39,40], together with the drop motion, which is taken into account using the standard Ranz and Marshall empirical mass transfer correlations for a moving sphere [41]; $1 + 0.3\,\text{Sc}^{1/3}\,\text{Re}^{1/2}$.

The external thermodynamical parameters are the humidity ratio in the air and the temperature in the whole system, which set the values of the evaporation parameter (see Ref. [13] for details). For the resolution of Eqs. (9) and (10), we consider water droplets evaporating in air. The air and water both are considered at 20 °C, and the humidity rate at infinity is taken at 80%. Solving this system leads to a shrinking droplet moving up and then back into the main liquid pool or to a complete evaporation in the air.

This simple model of Ghabache *et al.* [13] was shown to give accurate predictions of the experimentally observed, nontrivial trajectories of the evaporating droplets. These trajectories are

nontrivial because they depend on the variations of the drag force due to the varying size of the droplet as it evaporates. The good agreement with experimental trajectories thus indirectly validates the evaporation model in the context of the experiments of Ghabache *et al.* [13], i.e., laboratory conditions with water and ethanol solutions without air or water turbulent flows.

The simulations now provide all the necessary information on the droplet dynamics to use this simple evaporation model, i.e., the initial size and velocity of all ejected droplets. We obtain the total volume of evaporated liquid per droplet, e.g., for droplet i, $V_{d_i}^{\text{evap}}$. Figure 9(a) shows the evaporated volume for the first droplet, normalized by the initial volume of the first droplet, as a function of the Laplace and Bond number. We observe that for vanishing Bond number, the entire droplet is being evaporated. Then for higher Bond number, the normalized evaporated mass decreases as the Laplace number increases and seems to reach a constant value that depends on the Bond number. The Bond number has thus a crucial influence on the drop evaporation, probably due to the effect of gravity and the decrease in the ejection velocity.

Figures 9(b), 9(c), and 9(d) show, respectively, the evaporated volume of the second, third, and fourth droplets compared to the evaporated volume of the first drop. It shows, first, that, for Laplace number larger than 2000, the evaporated volume is smaller but stays comparable to the first one and varies with the control parameters following the same trend as the first drop, and, second, that, for $\text{La} < 2000$ the droplets $i > 1$ evaporate more than the first one. These results are important as they show that the evaporation of the subsequent droplets can not be neglected; the evaporation of the droplets following the first one is comparable to the first one and at La around 1000 it even becomes dominant.

These results are confirmed in Fig. 9(e), which shows the sum of the evaporated volumes of all the droplets compared to the first one $\sum_i V_{d_i}^{\text{evap}}/V_{d_1}^{\text{evap}}$, as a function of the control parameters. When there is more than just one ejected droplet, we observe that the volume loss by the first drop is at least twice smaller than the total evaporated volume. At Laplace close to 1000, it can even be several orders of magnitude larger. This effect decreases with increasing Bond number, in particular because the number of ejected droplets is reduced.

Finally, Fig. 9(f) shows the total evaporated volume for all the droplets normalized by total ejected volume, $\sum_i V_{d_i}^{\text{evap}}/(\frac{4}{3}\pi R_{di}^3)$. This figure further confirms that the Bond number mainly controls the ratio between the evaporated and ejected volume, while it appears almost independent of the Laplace number. Note that the influence of the Bond number is even stronger when the evaporation is summed over all the droplets than just considering the first one [Fig. 9(a)].

In order to further explore the influence of the control parameters on the total evaporated volume of the drops, it is plotted in Fig. 10(a) as a function of Laplace and Bond numbers, normalized by the initial bubble volume. We observe a strong Bond number dependency of the total evaporated volume, with an overall $\sum_i V_{d_i}^{\text{evap}}/V_{\text{bubble}} \propto \text{Bo}^{-1}$ as shown by the dashed line, with a weaker Laplace number dependence.

These scalings can be retrieved using the approximation proposed in Ghabache *et al.* [13]. We consider the limit case where the trajectory can be approximated by a parabola: $z(t) = v_d t - 1/2gt^2$ and $v_d = g\mathcal{T}_{\text{fly}}/2$ with $\mathcal{T}_{\text{fly}}$ the drop time of flight. Equation (10) can then be integrated between 0 and $\mathcal{T}_{\text{fly}}$ [13], and, introducing our nondimensional numbers, the normalized evaporated volume of the drop i can be approximated by

$$\frac{V_i^{\text{evap}}}{V_{\text{bubble}}} = 3\frac{\mu_{\text{air}}}{\mu_{\text{liq}}}\text{Sc}^{-1}\left(Y_{\text{vap}}^s - Y_{\text{vap}}^\infty\right)\text{La}^{-1}\frac{\text{La}_{d_i}\text{Ca}_i}{\text{Bo}}\left[1 + 0.3\text{Sc}^{1/3}\left(\frac{8}{9}\frac{\rho_{\text{air}}}{\rho_{\text{liq}}}\frac{\mu_{\text{liq}}}{\mu_{\text{air}}}\right)^{1/2}(\text{La}_{d_i}\text{Ca}_i)^{1/2}\right]. \quad (11)$$

In this equation $0.3\text{Sc}^{1/3}(\frac{8}{9}\frac{\rho_{\text{air}}}{\rho_{\text{liq}}}\frac{\mu_{\text{liq}}}{\mu_{\text{air}}})^{1/2}$ is much smaller than one for classical couples of liquid and gas (0.06 for water/air, or 0.09 for ethanol/air for instance). This suggests that evaporation does not depend much on droplet motion and allows us to neglect the second term: $(\text{La}_{d_i}\text{Ca}_i)^{1/2}$. Finally, this shows that the evaporated volume of an individual droplet scales as $\text{La}^{-1}(\text{La}_{d_i}\text{Ca}_i)/\text{Bo}$, thus retrieving the Bo^{-1} scaling observed numerically.

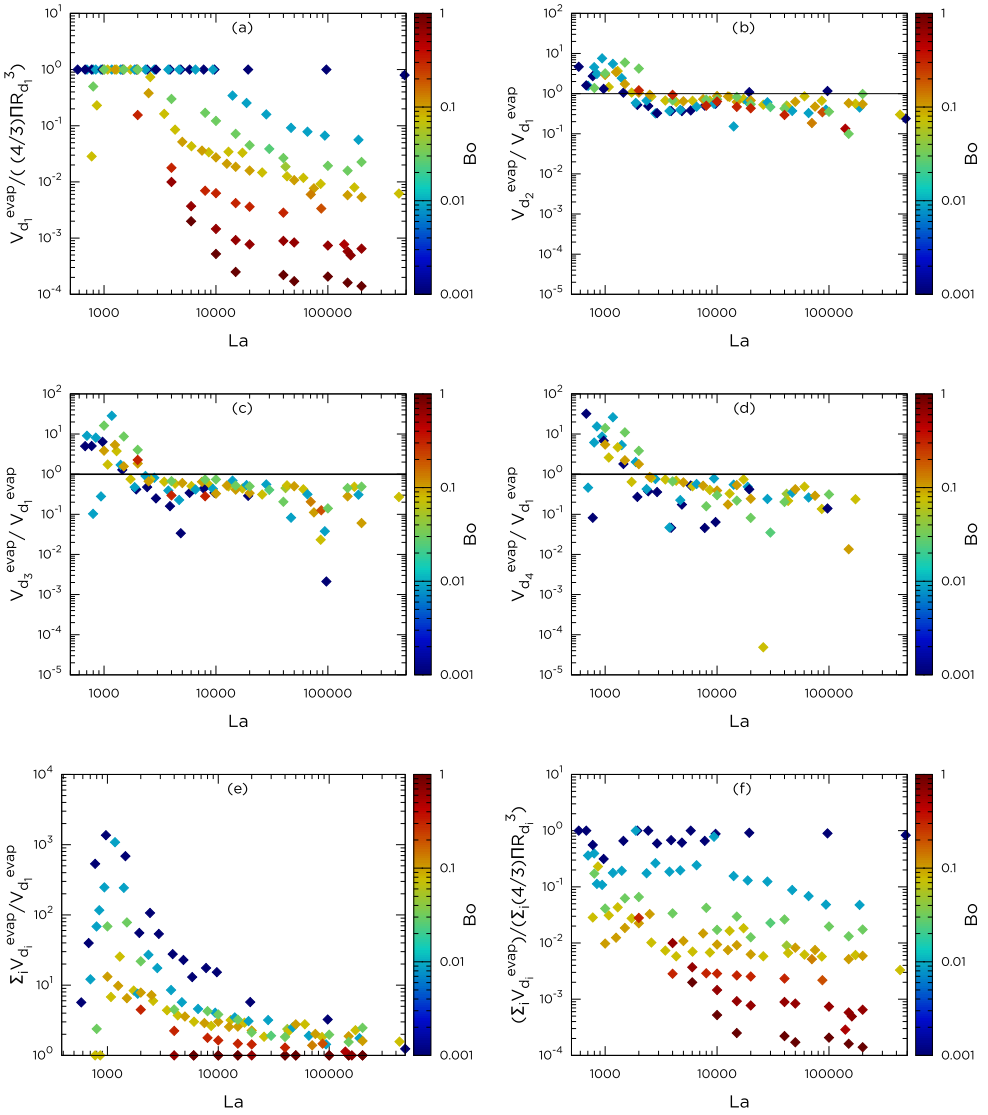

FIG. 9. (a) Evaporated volume of the first drop normalized by the ejected volume of the first drop, $V_{d_1}^{\text{evap}}/\frac{4\pi R_{d1}^3}{3}$ as a function of the Laplace number. For vanishing Bond number the total mass evaporates, while for large Laplace number and increasing Bond number, only a fraction of the ejected mass evaporates. (b) Evaporated volume of the second drop compared to the first one, $V_{d_2}^{\text{evap}}/V_{d_1}^{\text{evap}}$. The evaporated mass of the second droplet is comparable to the first one at high Laplace, and larger for La close to 1000, as a consequence of the results discussed regarding the droplet sizes. (c) and (d) Evaporated volume of the third and fourth drops compared to the first one, $V_{d_3}^{\text{evap}}/V_{d_1}^{\text{evap}}$ (c), and $V_{d_4}^{\text{evap}}/V_{d_1}^{\text{evap}}$ (d) showing similar results than the second droplet, with more scatter. (e) Total evaporated volume, $\sum_i V_{d_i}^{\text{evap}}$ normalized by $V_{d_1}^{\text{evap}}$ as a function of Bond and Laplace numbers. The total evaporated volume can be orders of magnitude larger than the evaporated volume from the first drop. This effect becomes less important for larger Bond number since increasing the Bond number both reduces the number of ejected droplets and the flight time of the droplets in the air. (f) Total evaporated volume compare to the total ejected volume in the air. For high Bond number, we evaporate all the liquid. As the Bond number increases, the volume that evaporates is smaller compared to the total ejected volume. The data suggest that this is independent from the Laplace number and that the only effect acting on the evaporated volume is the gravity, which controls the flight time of the droplet in the air.

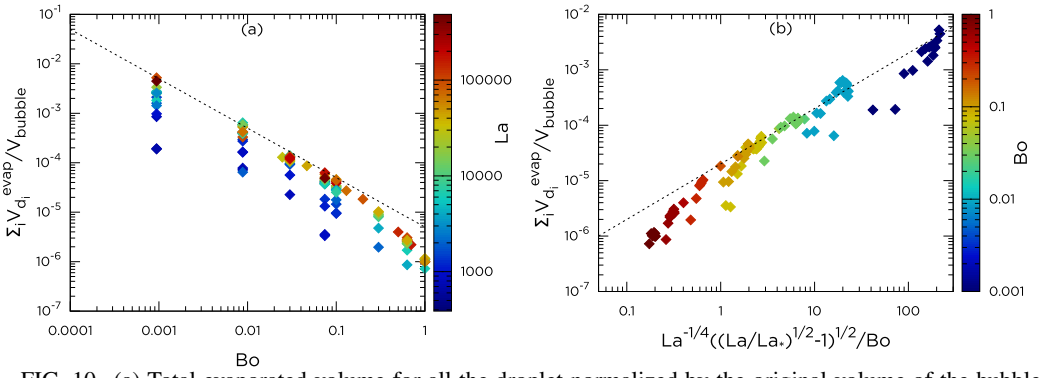

FIG. 10. (a) Total evaporated volume for all the droplet normalized by the original volume of the bubble $\sum_i V_{d_i}^{\text{evap}}/V_{\text{bubble}}$ as a function of the Bond number and the Laplace number (color-coded). This graph shows a high dependence in Bond number of the evaporated volume, $\propto \text{Bo}^{-1}$ (indicated with dashed line) and a small dependency with the Laplace number. (b) The total evaporated volume per bubble expressed as a function of our scaling: $[\text{La}^{-1/4}(\sqrt{\text{La}/\text{La}_*}-1)^{-1/2}/\text{Bo}$; see Eq. (12)], with a good collapse of the data on a 1:1 line except for the largest Bond number.

Now, by assuming that all droplets follow the same scaling as the first one, we can combine this expression of the evaporated volume with the scaling laws proposed by Gañàn-Calvo [19], and we obtain the following scaling for the total evaporated volume per bubble:

$$\sum_{i=1}^{N_{\text{drop}}} \frac{V_{di}^{\text{evap}}}{V_{\text{bubble}}} \sim \frac{\text{La}^{-1}\text{La}_{d_i}\text{Ca}_i}{\text{Bo}} \sim \frac{\text{La}^{-1/4}}{\text{Bo}}\left(\sqrt{\frac{\text{La}}{\text{La}_\star}}-1\right)^{1/2}. \tag{12}$$

Figure 10(b) presents $\sum_{i=1}^{N_{\text{drop}}} \frac{V_{di}^{\text{evap}}}{V_{\text{bubble}}}$ versus $\frac{\text{La}^{-1/4}}{\text{Bo}}(\sqrt{\frac{\text{La}}{\text{La}_\star}}-1)^{1/2}$ for the whole range of the bubble controlling parameters La and Bo. The points are reasonably consistent with a line of slope one, which confirms the validity of the scaling. This relation has direct practical interest since it gives a good estimation of the liquid volume evaporated when a bubble of a given size (Bo) bursts in a given liquid (La).

We note that in our simplified model the droplet velocity relative to the surrounding air is assumed to be identical to the velocity relative to the static free surface. In reality, the air surrounding the droplets is an ascending gas jet with a significant velocity in the vicinity of the axis. Numerical results indicate that the velocity of the droplet relative to the surrounding air can be up to 50% less than the absolute velocity, depending on its position in the sequence of ejected droplets. However, we have checked that these variations have only a minor influence on the total mass transfer estimated with our model.

Note also that the coupled modeling of the dynamics of the interfaces, temperature, and evaporation, while being possible in principle, is a challenging computational problem given the wide range of scales involved. Numerical schemes able to accurately perform this type of coupled thermodynamical modeling are a subject of active research. The relative simplicity of the (experimentally validated) evaporation-trajectory model used in the present study is at present an advantage, compared to the complexity and cost of such future DNS, as it allows one to investigate the effect of multiple droplets on the total evaporation rate, which happens at timescales much larger than the present simulated dynamics.

B. Applicability of the simple evaporation model for ocean-atmosphere applications

The evaporation model presented above does not take into account any small-scale atmospheric boundary layer above the surface. As such it is more representative of laboratory conditions with

essentially still air. The primary influence of an atmospheric boundary layer will be on the flight time of the eject droplets which is expected to increase. The evaporation should still be described by the d^2 relation, however. Indeed, the transport of the particle by the air flow will decrease the relative Reynolds number between the droplet and the air. The flight time could also be corrected according to the characteristics of the boundary layer and the droplet size as discussed by Refs. [32,42].

Note also that we do not consider the limiting effects of surface tension and salinity of the water, which limits evaporation for droplets smaller than 80 μm, these effects preventing complete evaporation of the droplets.

VI. CONCLUSIONS AND PERSPECTIVES

We have presented direct numerical simulations of jet droplets produced by bursting bubbles for a wide range of physical parameters summarised by the Laplace and Bond numbers. The results obtained for the first droplet confirm earlier numerical and experimental studies: The first droplet velocity decreases above an optimal Laplace number close to 1000 (which is Bond number dependent), while the first droplet size increases with a Laplace number above 1000 and is largely independent from the Bond number, except regarding the so-called optimal values, which are Bond dependent.

We then extended the numerical study to all the jet droplets produced by bubble bursting and discussed their number, size, and velocity as functions of the controlling parameters. We observe a systematic reduction of the droplet velocity as their production number increases. The size of the subsequent droplets vary by less than an order of magnitude except in the case of Laplace numbers close to 1000 at vanishing Bond numbers, where the fastest and thinnest jets are produced. These cases also correspond to the largest numbers of ejected droplets. The ejection process of the subsequent droplets present some internal variability, which should be studied systematically with a statistical analysis. The present extensive numerical data set will nurture the active debate on the theoretical scalings for the number, size, and velocity proposed in the literature and the exact physical interpretation of the underlying mechanism for various Laplace numbers [19–21,29,34], while also providing critical quantitative data on the relative importance of jet and film drops in ocean spray production [23,32].

The total vertical momentum of the ejected droplets is shown to follow a simple $\mathrm{La}^{1/2}$ scaling for low enough Bond numbers and above the optimal Laplace number (1000), which is an interesting result when considering air-sea momentum fluxes.

Combining these numerical results with a relatively simple evaporation model, we demonstrated that all the jet droplets play a significant role in the total amount of water evaporated during a single bubble bursting event, in contrast with what was assumed in previous studies where only the first droplet was considered. We also obtained a simple scaling relationship, consistent with the simplified evaporation model, which describes the total amount evaporated as a function of the bubble size and fluid properties.

The various scalings and results were obtained considering an idealized configuration of a single bubble bursting in a quiescent liquid, neglecting various effects which could be of importance under realistic ocean-atmosphere conditions, such as the influence of the wave field, the turbulent boundary layers in the air or water, collective effects, or complex physico-chemistry of the interface induced by surfactants. The evaporation model we use also presents limitations in the case of sea water which would need to be considered when applying the proposed framework to ocean spray.

ACKNOWLEDGMENTS

This work was supported by the National Science Foundation under Grant No. 1849762 to L.D. and the Cooperative Institute for Earth System modeling between Princeton and GFDL NOAA. A.B. was supported by the International Fund to L.D. from Princeton University during part of this study.

[1] A. H. Woodcock, C. F. Kientzler, A. B. Arons, and D. C. Blanchard, Giant condensation nuclei from bursting bubbles, Nature (London) **172**, 1144 (1953).
[2] C. F. Kientzler, A. B. Arons, D. C. Blanchard, and A. H. Woodcock, Photographic investigation of the projection of droplets by bubbles bursting at a water surface, Tellus **6**, 1 (1954).
[3] D. C. Blanchard, Bursting of bubbles at an air-water interface, Nature (London) **173**, 1048 (1954).
[4] D. C. Blanchard and A. H. Woodcock, Bubble formation and modification in the sea and its meteorological significance, Tellus **9**, 145 (1957).
[5] D. C. Blanchard, The electrification of the atmosphere by particles from bubbles in the sea, Progr. Oceanogr. **1**, 73 (1963).
[6] D. C. Blanchard and L. Syzdek, Mechanism for the water-to-air transfer and concentration of bacteria, Science **170**, 626 (1970).
[7] D. E. Spiel, The number and size of jet drops produced by air bubbles bursting on a fresh water surface, J. Geophys. Res. **99**, 10289 (1994).
[8] D. E. Spiel, More on the births of jet drops from bubbles bursting on seawater surfaces, J. Geophys. Res. **102**, 5815 (1997).
[9] G. Liger-Belair, How many bubbles in your glass of bubbly? J. Phys. Chem. B **118**, 3156 (2014).
[10] T. Séon and G. Liger-Belair, Effervescence in champagne and sparkling wines: From bubble bursting to droplet evaporation, Eur. Phys. J.: Spec. Top. **226**, 117 (2017).
[11] L. Duchemin, S. Popinet, C. Josserand, and S. Zaleski, Jet formation in bubbles bursting at a free surface, Phys. Fluids **14**, 3000 (2002).
[12] E. Ghabache, A. Antkowiak, C. Josserand, and T. Séon, On the physics of fizziness: How bubble bursting controls droplets ejection, Phys. Fluids **26**, 121701 (2014).
[13] E. Ghabache, G. Liger-Belair, A. Antkowiak, and T. Séon, Evaporation of droplets in a Champagne wine aerosol, Sci. Rep. **6**, 25148 (2016).
[14] E. Ghabache and T. Séon, Size of the top jet drop produced by bubble bursting, Phys. Rev. Fluids **1**, 051901(R) (2016).
[15] S. Popinet, An accurate adaptive solver for surface-tension-driven interfacial flows, J. Comput. Phys. **228**, 5838 (2009).
[16] S. Popinet, Numerical models of surface tension, Annu. Rev. Fluid Mech. **50**, 49 (2018).
[17] L. Deike, E. Ghabache, G. Liger-Belair, A. K. Das, S. Zaleski, S. Popinet, and T. Séon, Dynamics of jets produced by bursting bubbles, Phys. Rev. Fluids **3**, 013603 (2018).
[18] C. F. Brasz, C. T. Bartlett, P. L. L. Walls, E. G. Flynn, Y. E. Yu, and J. C. Bird, Minimum size for the top jet drop from a bursting bubble, Phys. Rev. Fluids **3**, 074001 (2018).
[19] A. M. Gañán-Calvo, Revision of Bubble Bursting: Universal Scaling Laws of Top Jet Drop Size and Speed, Phys. Rev. Lett. **119**, 204502 (2017).
[20] A. M. Gañán-Calvo, Scaling laws of top jet drop size and speed from bubble bursting including gravity and inviscid limit, Phys. Rev. Fluids **3**, 091601(R) (2018).
[21] J. M. Gordillo and J. Rodríguez-Rodríguez, Capillary waves control the ejection of bubble bursting jets, J. Fluid Mech. **867**, 556 (2019).
[22] C.-Y. Lai, J. Eggers, and L. Deike, Bubble Bursting: Universal Cavity and Jet Profiles, Phys. Rev. Lett. **121**, 144501 (2018).
[23] H. Lhuissier and E. Villermaux, Bursting bubble aerosols, J. Fluid Mech. **696**, 5 (2012).
[24] http://basilisk.fr/sandbox/aberny/bubble/bubbleShape.h.
[25] http://basilisk.fr.
[26] L. Deike, S. Popinet, and W. K. Melville, Capillary effects on wave breaking, J. Fluid Mech. **769**, 541 (2015).
[27] L. Deike, W. K. Melville, and S. Popinet, Air entrainment and bubble statistics in breaking waves, J. Fluid Mech. **801**, 91 (2016).
[28] L. Deike, L. Lenain, and W. K. Melville, Air entrainment by breaking waves, Geophys. Res. Lett. **44**, 3779 (2017).
[29] A. M. Ganán-Calvo and J. M. Lopez-Herrera, Capillary soft singularities and ejection: Application to the physics of bubble bursting, arXiv:1911.08844.

[30] E. Ghabache, Surface libre hors équilibre: de l'effondrement de cavité aux jets étirés, Ph.D. thesis, Université Pierre et Marie Curie – Paris VI, 2015.
[31] P. L. L. Walls, L. Henaux, and J. C. Bird, Jet drops from bursting bubbles: How gravity and viscosity couple to inhibit droplet production, Phys. Rev. E **92**, 021002 (2015).
[32] F. Veron, Ocean spray, Annu. Rev. Fluid Mech. **47**, 507 (2015).
[33] L. Deike and W. K. Melville, Gas transfer by breaking waves, Geophys. Res. Lett. **45**, 10,482 (2018).
[34] F. J. Blanco-Rodríguez and J. M. Gordillo, On the sea spray aerosol originated from bubble bursting jets, J. Fluid Mech. **886**, R2 (2020).
[35] W. A. Sirignano, *Fluid Dynamics and Transport of Droplets and Sprays* (Cambridge University Press, Cambridge, UK, 1999).
[36] A. Frohn and N. Roth, *Dynamics of Droplets*, softcover repr. of hardcover 1st ed. (2000 ed.), Engineering Online Library (Springer, Berlin, 2010).
[37] R. Clift, J. R. Grace, and M. E. Weber, *Bubbles, Drops, and Particles*, Dover Books on Engineering (Dover, New York, 2005).
[38] Z. Naumann and L. Schiller, A drag coefficient correlation, Z. Ver. Deutsch. Ing. **77**, 318 (1935).
[39] I. Langmuir, The evaporation of small spheres, Phys. Rev. **12**, 368 (1918).
[40] N. A. Fuchs, *Evaporation and Droplet Growth in Gaseous Media* (Pergamon, London, 1959).
[41] W. Ranz and W. R. Marshall, Evaporation from drops, Chem. Eng. Prog. **48**, 141 (1952).
[42] E. L. Andreas, J. B. Edson, E. C. Monahan, M. P. Rouault, and S. D. Smith, The spray contribution to net evaporation from the sea: A review of recent progress, Bound.-Layer Meteorol. **72**, 3 (1995).